METEOROLOGICAL APPLICATIONS
Meteorol. Appl. **21**: 910–921 (2014)
Published online 6 November 2013 in Wiley Online Library
(wileyonlinelibrary.com) DOI: 10.1002/met.1431

RMetS
Royal Meteorological Society

Large-eddy simulation of an offshore Mediterranean area

Umberto Rizza,[a]* Mario M. Miglietta,[a] Anna M. Sempreviva,[b,c] Fabio Grasso[a] and M. Elisabetta Schiano[d]

[a] *CNR ISAC, Unit of Lecce, Italy*
[b] *CNR ISAC, Unit of Lamezia, Italy*
[c] *Wind Energy Department, Danish Technical University, Roskilde, Denmark*
[d] *CNR/ISMAR, Unit of Genoa, Italy*

ABSTRACT: The aim of this study is to gain further understanding of the structure of the marine atmospheric boundary layer (MABL) and its interaction with synoptic-scale forcing. A possible application of this study is to simulate mean and turbulent spatial and temporal structure of the marine boundary layer in order to optimize the structural design of offshore large wind turbines that today reach heights up to 200 m. Large-eddy simulations (LESs) have been performed and compared with offshore experimental data collected during the LASIE campaign performed in the Mediterranean during summer 2007. Two simulations are performed: one where the LES is left free to evolve without any external forcing, and one where a force restoration nudging technique has been implemented in LES in order to force the model to the evolving large-scale situation. Model results have been compared against experimental soundings. Results show that for all the calculated fields the nudged LES outperforms the simulation without nudging, demonstrating that incorporating changes in the large-scale features is necessary in order to provide a realistic evolution of the modelled meteorological fields at local scale. Thus, appropriately nudged LES appears as a promising technique to be applied to the simulation of offshore cases, particularly suitable for wind energy applications.

KEY WORDS offshore LES; MABL; offshore wind farms

Received 23 January 2013; Revised 28 March 2013; Accepted 16 July 2013

1. Introduction

The European Wind Energy Association (EWEA) estimates that electricity production from wind power will increase from 182 Terawatt hours (TWh) or 5.5% of the total EU demand in 2010, to 581 TWh or 17.5% of the total demand in 2020. Within this context, an increasingly part of the energy production will be generated from offshore wind farms. The interest for planning offshore wind farms is growing, since they have some undisputed advantages with respect to onshore locations, i.e. wind is more intense and less turbulent over sea than over land and the social acceptance is a minor issue with respect to inland installations. New generations of offshore wind turbine tips are reaching up to 200 m and this value will keep growing in the future.

For the optimal exploitation of wind resources (i.e., to optimize turbine design and wind farms layouts), it is of paramount importance to study offshore wind conditions especially with respect to vertical profiles of wind and turbulence. However, there are still gaps in understanding the variability of vertical mean wind and turbulence profiles at such heights and in such a harsh environment. As a consequence, the installation of tall offshore masts aimed at characterizing areas of interest for prospective wind farms is not economically sustainable. Innovative measuring systems such as floating LIDAR, i.e. Leosphere FLIDAR©, have been developed, but these devices are very expensive and offshore wave conditions pose logistical issues.

* Correspondence: U. Rizza, CNR ISAC, Unit of Lecce, Lecce 73100, Italia. E-mail: u.rizza@isac.cnr.it

Furthermore, the study of the evolution of the mean and turbulent vertical structure of the Marine Atmospheric Boundary Layer (MABL) nearby coastal and offshore areas is one of the most challenging issues in meteorology. An Internal Boundary Layer (IBL) develops from the coastal discontinuity caused by a step variation in surface temperature, moisture and roughness and ultimately merges with the MABL far from the coastline. The evolution of the coastal MABL depends on the direction of the air flowing over it, and hence on the large-scale circulation, i.e. on offshore or onshore winds, in a non-trivial way.

When the wind blows onshore the offshore profiles are usually in equilibrium with the sea surface. On the other hand, offshore flow takes some distance from the coast to reach an equilibrium depending on the temperature difference between sea surface and the air flowing over it (Pryor and Barthelmie, 2002; Lange *et al.*, 2004; Barthelmie *et al.*, 2005). This is especially of interest in enclosed seas where the fetch coast to coast might be too short for the flow to reach an equilibrium with the surface.

An important case occurs during so-called cold-air outbreaks, when cold air flows over a warm water surface causing an intense change in air properties, often followed by severe weather phenomena such as strong convection and heavy precipitation. Warm continental air advected over a cold sea surface also produces intense changes in air properties, even if the modified MABL is much shallower. Turbulence in this stably stratified layer may be considerably reduced: the resulting weakly convective boundary layer is generally decoupled from the surface (Skyllingstad *et al.*, 2005) and in some cases fog formation may reduce the visibility. Garratt and Ryan (1989) studied the development of a stable Internal Boundary-Layer (IBL) off the coast of southeast Australia, during an outbreak of

warm and dry air from land. Their conclusion was that a stable IBL might be found at distances up to 300 km from the coast, estimating ground-based inversions at three different points from radiosoundings and aircraft measurements. Sempreviva *et al.* (2010) found a similar situation in a case study during the LASIE (Ligurian Air-Sea Interaction Experiment) experimental campaign in the Mediterranean (Teixeira, 2007).

To characterize the evolution of the vertical structure of the MABL from the surface to its top, extensive meteorological and oceanographic observations must be carried out *in situ* either using ship- and buoy-based platforms or using remote sensing devices. Unfortunately, there are only few complete available databases because of logistics and environmental constraints coupled to the high costs of intensive campaigns. Therefore, most of the studies have been carried out mainly from coastal locations at the shoreline and/or from islands (Sempreviva and Gryning, 2000; Edson *et al.*, 2007; Helmis, 2007; Smedman *et al.*, 2007).

In real cases the evolution of the vertical structure of the MABL is quite complex and is driven by a combination of processes at different spatial-temporal scales such as synoptic forcing, cloud cover, ambient turbulence. An innovative approach to tackle with this problem is using turbulence-resolving high-resolution methodologies such as LES coupled to mesoscale models. In fact LES describes local processes and is usually driven by surface processes, without including the evolution at the large scale. Therefore, a delicate question regarding MABL-LES is the inclusion of synoptic forcing within the LES. In the study of realistic cases, where the flow is driven by larger scale forcing, one approach is to represent the forcing from atmospheric processes larger than the LES domain scale by introducing additional terms in the LES equations (Conzemius, 2004). In this context, the recent work of Conzemius and Fedorovich (2010) depicted that the force-restore nudging provided a realistic reproduction of the LES mean wind, temperature and humidity profiles when compared with the corresponding vertical profiles of the IHOP (International H_2O Project) field experiment (Weckwerth *et al.*, 2004). Similar studies were also performed recently (Basu *et al.*, 2008; Kumar *et al.*, 2010; Pedersen *et al.*, 2012).

To the authors' knowledge, there are few applications of LES in offshore sites, and these are mainly dedicated to the study of a cloud topped MABL under idealized forcing conditions (Stevens, 2005). In a recent paper Sullivan *et al.* (2008) have examined the interaction between atmospheric turbulence and swell, using an LES model developed with the capability of imposing propagating sinusoidal modes at its lower boundary. LES results illustrate the importance of wave phase speed relative to wind speed and the relative orientation of winds and waves. Bulk parameterizations of the surface drag need to account for the wave state. Also, the work of Cañadillas *et al.* (2010) can be mentioned, in which an idealized LES has been used and compared with offshore observational data taken at the FINO1 offshore platform in the North Sea. The authors found a good qualitative agreement of model simulations with data: the differences can be mostly explained with the sensitivity to the initial conditions.

The goal of the present study is to test the implementation of the force-restore nudging in a turbulence-resolving large-eddy simulation applied to a real case. This nudging is implemented using the LASIE database (Teixeira, 2007) in the Mediterranean Sea. This experiment was designed to provide an additional dataset to the few available in the area, including comprehensive air-sea measurements under different synoptic conditions. The validity of the force-restore nudging has been tested using two different LES runs with different setup and compared with the measured vertical profiles of mean wind, temperature and humidity.

2. Experimental setup

2.1. The LASIE dataset

A complete description of the LASIE experiment (16–22 June 2007) including the experimental setup and the observed atmospheric conditions can be found in Sempreviva *et al.* (2010) and Small *et al.* (2011). The main purpose of LASIE was to improve the evaluation and development of parameterization schemes of PBL, providing a general strategy in the atmospheric modelling community. This was planned through a detailed characterization of the mean and turbulent structure of ocean/atmosphere boundary layers in the Ligurian Sea, using: observations taken from ships (*Planet*, *Urania* and *Leonardo*), two CNR and ENEA meteo-oceanographic buoys, and the remote sensing capabilities at NURC.

Here, the conditions on 21–22 June 2007 are considered, when the MABL has been intensively monitored using different instrumentation devices installed on different measuring platforms. A limited dataset functional to the presented simulation study is used. The data are taken from two measuring platforms owned by the Italian National Research Council (CNR) i.e. the buoy ODAS-Italia1 (Nittis *et al.*, 2007), and the research vessel N/O *Urania*. On the buoy, positioned in the Ligurian Sea (Figure 1), atmospheric and marine standard measurements are regularly collected at different frequencies: wind speed U ($m\,s^{-1}$) and wind direction DIR ($^\circ$); radiation R ($W\,m^{-2}$); air temperature Ta ($^\circ$C), atmospheric pressure P (hPa) and relative humidity RH (%). The URANIA research vessel sailed along different tracks. Beside standard meteorological and turbulence measurements, vertical profiling of the Marine Atmospheric Boundary Layer was performed by radiosondes (DigiCORA Sounding MW21 System) released every 3 h, and recording vertical profiles of U, DIR, T_p (potential temperature) and RH. Vertical profiles are used in this study for comparison with the LES output.

2.2. Synoptic analysis

Large-scale conditions are discussed in the present subsection, considering the reanalysis maps of the NCEP – NCAR (National Centre for Atmospheric Research – National Centre for Environmental Prediction; plotted from the web page at the Physical Sciences 12 Division (PSD) of the NOAA/Earth System Research Laboratory) 40 year Reanalysis Project (NNRP; Kalnay *et al.*, 1996). The horizontal resolution of the reanalysis data is about 2.5 $^\circ$, and thus it is only appropriate to represent the large-scale features.

The synoptic maps show a quasi-stationary ridge, slowly moving eastward from 18 to 22 June over the central Mediterranean basin. On 20 June this high-pressure feature extends from Tunisia to Italy, with its extreme northern part affecting Norway (Figure 2). As a consequence, a pressure minimum located on its western side, which is present both at low and upper levels, is prevented from moving eastward, and remains confined close to the British Isles, where it progressively weakens in the following days. The Ligurian Sea appears close to the main axis of the ridge, slightly to the west, and is affected by a weak south-westerly flow. At low levels, a relatively high,

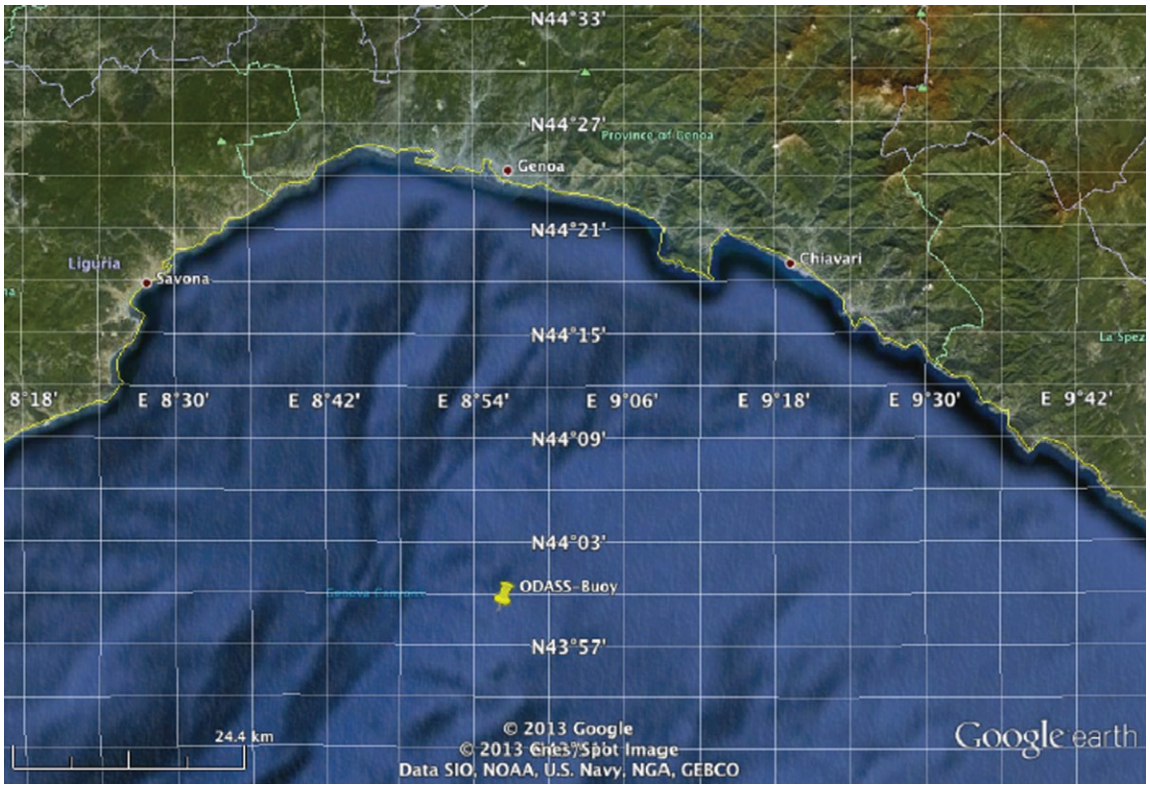

Figure 1. The operational area of the N/O *Urania* research vessel during LASIE and the position of the buoy ODASS-Italia 1 (© 2013 Google, © 2013 Cnes/Spot Image). This figure is available in colour online at wileyonlinelibrary.com/journal/met

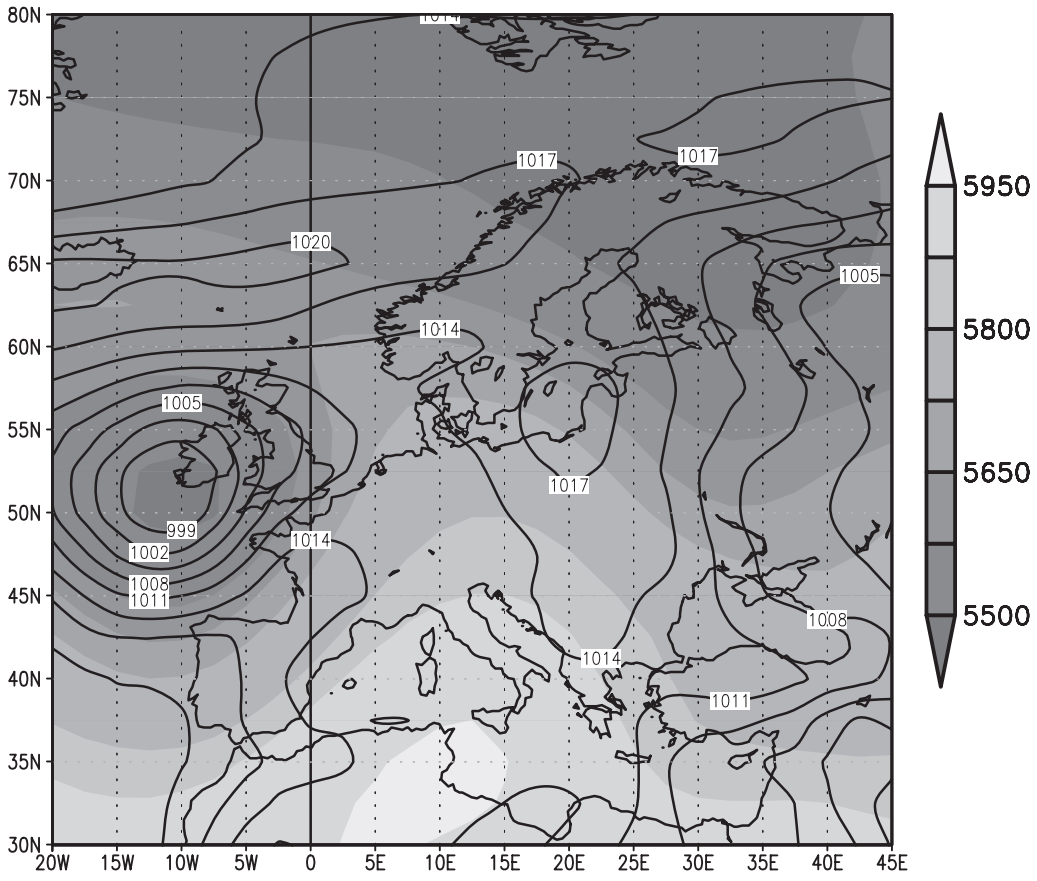

Figure 2. NCEP reanalysis maps, daily composite mean on 20 June 2007: 500 hPa geopotential height (in gpm) and mean sea level pressure (hPa).

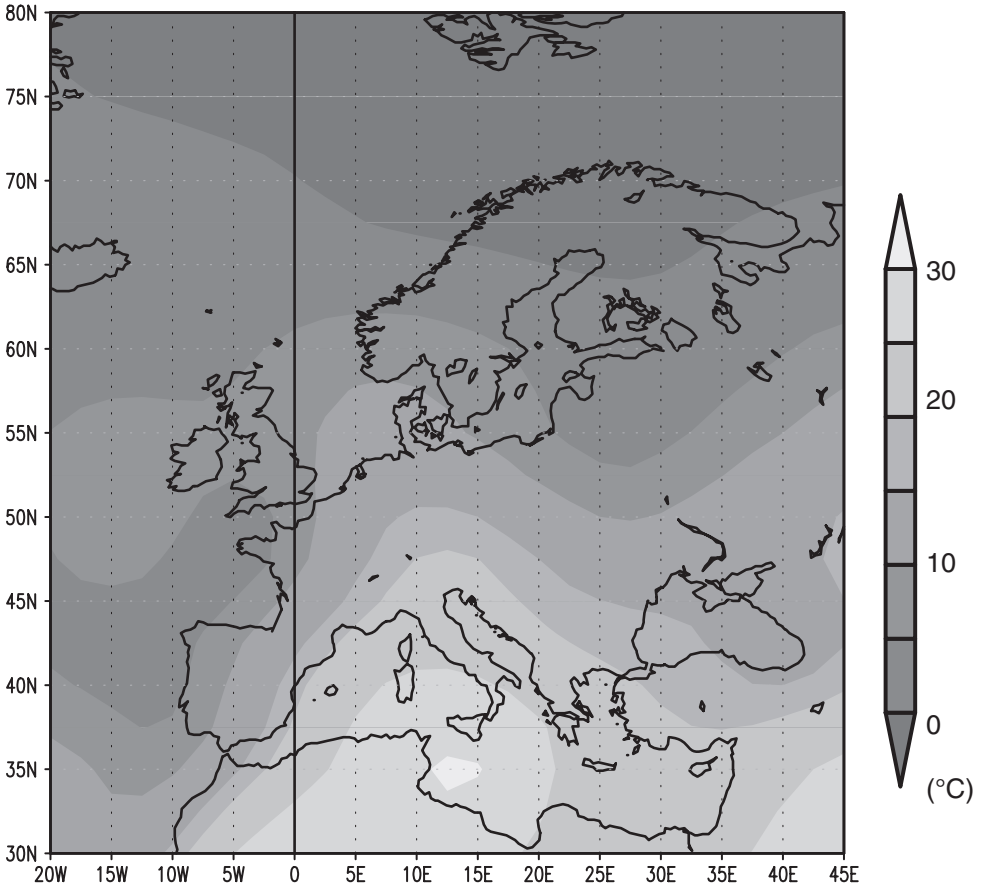

Figure 3. NCEP reanalysis maps, daily composite mean on 20 June 2007: 850 hPa temperature (°C).

levelled pressure field covers the central Mediterranean basin, determining a weak circulation in the area. The high pressure configuration is associated with a tongue of very warm air extending from northern Africa (Figure 3) towards Europe. Its hottest part reaches Sicily, with 850 hPa temperatures of 30 °C on 21 June. The thermal ridge crosses the Ligurian sea on 20 June, with 850 hPa temperature above 20 °C. The low relative humidity associated with the air mass prevents the formation of significant cloud cover in the Mediterranean basin.

3. The Large-Eddy Model

3.1. Model description and settings

In this paper the NCAR (National Centre Atmospheric Research) large-eddy model (Moeng, 1984) is used. It exploits the incompressible Boussinesq form of the Navier–Stokes equations for a horizontally homogeneous boundary layer. The code solves the filtered continuity equation, the filtered momentum conservation equation, and the filtered heat transport equation:

$$\frac{\partial \overline{u}_i}{\partial x_i} = 0$$
$$\frac{\partial \overline{u}_i}{\partial t} + \overline{u}_j \frac{\partial \overline{u}_i}{\partial x_j} = -\frac{\partial P^*}{\partial x_i} - \frac{\partial \tau_{ij}}{\partial x_j} + \delta_{i3} g \frac{\overline{\theta} - <\overline{\theta}>}{\theta_0} + f_c \epsilon_{ij3} \overline{u}_j$$
$$\frac{\partial \overline{\theta}}{\partial t} + \overline{u}_j \frac{\partial \overline{\theta}}{\partial x_j} = -\frac{\partial q_j}{\partial x_j} \qquad (1)$$

where τ is the Reynolds stress, $< \overline{\theta} >$ is the planar average of potential temperature, g is the gravitational acceleration, f_c is the Coriolis parameter and q_j is the subgrid (SGS) heat flux. The modified pressure term P^* is written as $\overline{p} + 1/2\ \rho \overline{u}_i \overline{u}_j$, in this way the mean horizontal pressure gradient force term ($\overline{p}$) may be related with the geostrophic wind components (U_g,V_g):

$$\frac{\partial \overline{p}}{\partial x} = -fV_g$$
$$\frac{\partial \overline{p}}{\partial y} = fU_g \qquad (2)$$

The relations among SGS for the velocity and temperature fields are given by:

$$\tau_{ij} - \frac{1}{3}\ \tau_{kk}\ \delta_{ij} = -2K_M \left(\frac{\partial u_i}{\partial x_j} + \frac{\partial u_j}{\partial x_i}\right) \qquad (3)$$

$$q_j = -\frac{K_M}{PR_{sgs}} \frac{\partial \overline{\theta}}{\partial x_j} \qquad (4)$$

where $(i, j) = (x, y, z)$, K_M is the eddy viscosity coefficients and PR_{sgs} is the SGS Prandtl number. A usual way of modelling the eddy-viscosity coefficient for the momentum K_M is given by:

$$K_M = 0.1\ l\ \left(\overline{e'}\ \right)^{1/2} \qquad (5)$$

where l is the mixing length and $\left(\overline{e'}\ \right)^{1/2}$ is a turbulent velocity scale obtained from the SGS energy budget equation.

Table 1. LES settings.

Acronym	LES-FR	LES-NOFR
Domain extension	(5, 5, 2) km	(5, 5, 2) km
Grid points	(128, 128, 192)	(128, 128, 192)
Start time	20 June 2007 at 1000 Z	20 June 2007 at 1000 Z
End time	21 June 2007 at 0000 Z	21 June 2007 at 0000 Z
Geostrophic forcing	Baroclinic	Baroclinic
Force-restore nudging	Yes	No

Additional features, including boundary conditions of the LES model, can be found in Moeng (1984).

It is important to mention that this specific LES code has been extensively used and tested to study many aspects of the Planetary Boundary-Layer (PBL) flows (e.g., Moeng, 1984; Moeng and Sullivan, 1994; Saiki *et al.*, 2000; Antonelli *et al.*, 2003; Anfossi *et al.*, 2006; Rizza *et al.*, 2010).

The LES domain is confined around the ODAS Italia-1 spar buoy that is moored about 73 km south of Genoa (Sempreviva *et al.*, 2010). Homogeneous surface fluxes are assumed within the LES domain that has a horizontal extension of 5×5 km.

Realistic settings for LES must consider a variation of the surface heat flux that reproduces the intensity of the solar heating in offshore sites (as explained in Section 3.2), the variation with height of the wind intensity, a baroclinic geostrophic wind profile and the inclusion of large-scale effects obtained from experimental profiles. All of these aspects have been considered in the present investigation. In this context, two different simulations have been performed, with two different ways for incorporating the large-scale advection in LES. Table 1 reports the LES settings employed for the two simulations. The horizontal domain has an extension of 5×5 km with 128^2 grid points. The vertical extension is 2 km with 192 grid points. The corresponding grid cell resolution is $39 \times 39 \times 10.5$ m. Both LES runs started at 1000 UTC (0900 LST) on 20 June, in correspondence with the radio-soundings launched at the ship main deck, and ran for approximately 15 h. The difference between the two runs mainly consists on the way the large-scale advection is incorporated within the LES code.

3.2. Initial conditions and surface forcing

The initial profiles of specific humidity, potential temperature and wind components are obtained interpolating into the LES-grid the soundings taken at 0900 LST, 20 June (Sempreviva *et al.*, 2010). These profiles are shown in Figure 4. The potential temperature has a typical stable profile characterized by a low surface inversion (3K over the lowest 50 m).

PBL flows are driven by an imposed surface heat flux or a temperature gradient near the surface. Surface fluxes of temperature and moisture are calculated from measured sensible (SHF) and latent heat (LHF) fluxes as:

$$\overline{w'\theta'} = \frac{SHF}{\rho C_p} \tag{6}$$

$$\overline{w'q'} = \frac{LHF}{\rho L_v} \tag{7}$$

$$\overline{w'\theta'_v} = \overline{w'\theta'} + 0.61\theta_{v0}\ \overline{w'q'} \tag{8}$$

In the above expressions, ρ is the density of air, C_p is the specific heat, L_v is the latent heat of vapourization, $w'\theta'$ is the surface kinematic temperature flux, $\overline{w'q'}$ is the surface kinematic humidity flux and θ_{v0} is the surface reference virtual temperature.

Both LES runs were forced with the surface kinematic temperature flux $\overline{w'\theta'_v}$ (Figure 5(a)) and the surface kinematic moisture flux $\overline{w'q'}$ (Figure 5(b)).

Two important contrasting features can be noticed in comparison with the land case. First, the intensity of $\overline{w'\theta'_v}$ is quite weak during the whole day: the maximum occurs at 1800 LST with the corresponding value less than 10 W m^{-2}. Second, the well defined over-land daily cycle is not present in this offshore site. The analysis of Figure 6 also indicates that during the simulated period the MABL is in condition of very weak convective or almost neutral conditions.

3.3. The large-scale pressure gradient

Assuming the geostrophic balance, the large-scale pressure gradient can be associated with the components of the geostrophic wind (U_g, V_g). The LES model was forced with a time varying baroclinic geostrophic setup that is consistent with that derived from a simulation using the Advanced Research-Weather Research and Forecasting (WRF-ARW) model (Skamarock *et al.*, 2008). The geostrophic forcing within the LES is applied hour by hour in correspondence of the frequency of the WRF output fields. This coupling corresponds to a one-way nesting between the WRF model and the actual LES code (Rizza *et al.*, 2013). Actually, the authors are aware of relatively few studies of the PBL using the WRF model in Mediterranean coastal and offshore domains (e.g., De Tomasi *et al.*, 2011; Miglietta *et al.*, 2013).

The WRF model simulation starts at 0000 UTC on 19 June 2007 and lasts for 72 h. The large-scale initial and boundary conditions (updated every 6 h) are provided by the Global Forecasting System (GFS) analyses. Two domains are two-way nested, employed with horizontal resolutions of 12 and 3 km respectively. The number of grid points is, respectively, 111×111, and 133×133, centred in correspondence with the buoy location: 28 vertical levels are implemented. The parameterization schemes selected are: WRF single moment (WSM) 3-class simple ice scheme; the rapid radiative transfer model (RRTM) for longwave and the Dudhia scheme for short wave radiation; the Monin-Obukhov (Janjic) scheme for the surface layer and the Mellor-Yamada-Janjic TKE scheme for the boundary layer; the Unified Noah for the land-surface model; the Kain-Fritsch (new Eta) cumulus scheme, and the horizontal Smagorinsky first order closure for diffusion. It was verified that the WRF model simulation is able to capture the large scale features well.

Figure 7 depicts the height-time plot of the geostrophic wind components. This is equivalent to specifying a time-varying large-scale pressure gradient. The incorporation of the evolution of the large-scale pressure gradient represents an improvement of the LES prognostic capability as denoted by Conzemius and Fedorovich (2008a) and Rizza *et al.* (2013).

3.4. The force-restore nudging

In the marine environment, due to the high thermal capacity of the water body, the surface fluxes and the evolution of the vertical structure of the MABL depend on several factors, such as the geographic location and the synoptic conditions. In this context, it is fundamental to represent the large-scale forcings in LES. One common approach is to represent the forcing from atmospheric processes larger than the LES domain scale

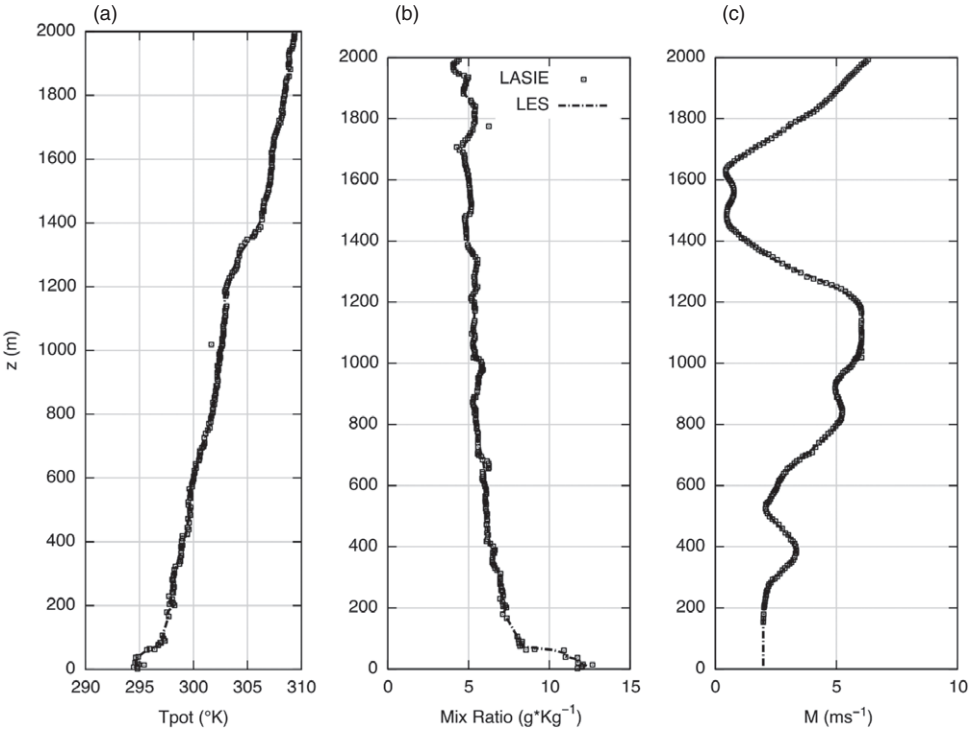

Figure 4. Initial profiles for LES of potential temperature (a), Mixing ratio (b) and wind speed (c) taken from experimental soundings at 1000 UTC, 20 June.

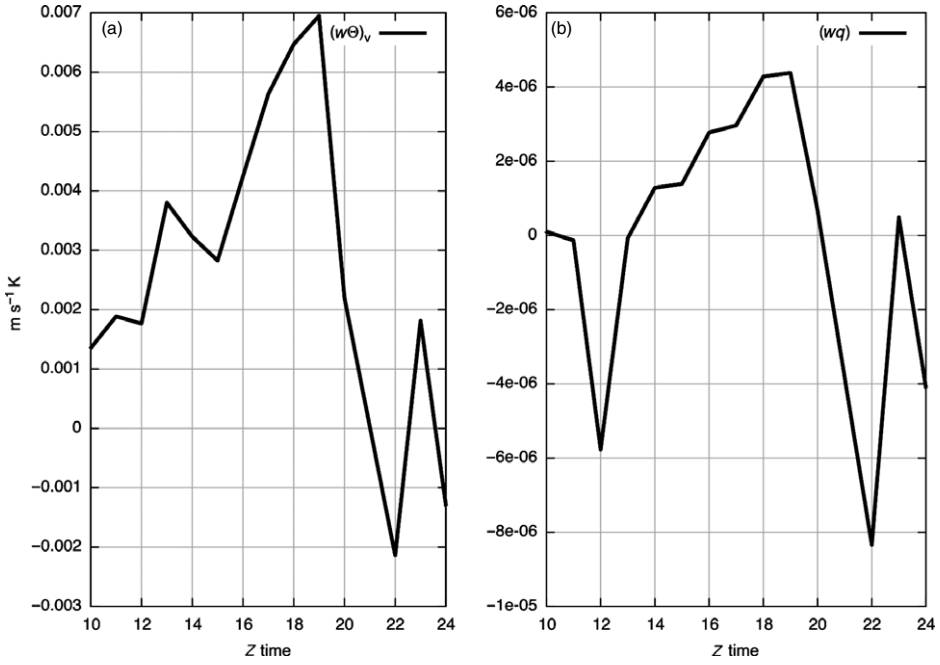

Figure 5. Time series of the surface kinematic temperature flux (a) and the surface kinematic moisture flux (b) during 20 June.

by using additional terms in the LES equations (Conzemius, 2004). Conzemius and Fedorovich (2010) have tested three methods: (1) time-constant large-scale pressure gradient force; (2) time-varying large-scale pressure gradient plus advection; (3) time-varying large-scale pressure gradient plus a force-restore method.

As described in the previous chapter, the Coriolis and large-scale pressure gradients (represented as geostrophic wind vectors) were updated hourly based on the outputs of model WRF around the area of interest as in Rizza *et al.* (2013). The force-restore method described in Gibbs *et al.* (2011) was used as follows:

$$\frac{\partial \overline{\Phi}(z)_{\mathrm{LES}}}{\partial t} = -\frac{\overline{\Phi}(z)_{\mathrm{LES}} - \overline{\Phi}(z)_{\mathrm{LASIE}}}{t_R} \tag{9}$$

where $\overline{\Phi}$ is the considered resolved flow variable, and t_{R} is the nudging time constant, that, consistently with the time interval between two radio-soundings, was set equal to 3 h. The right

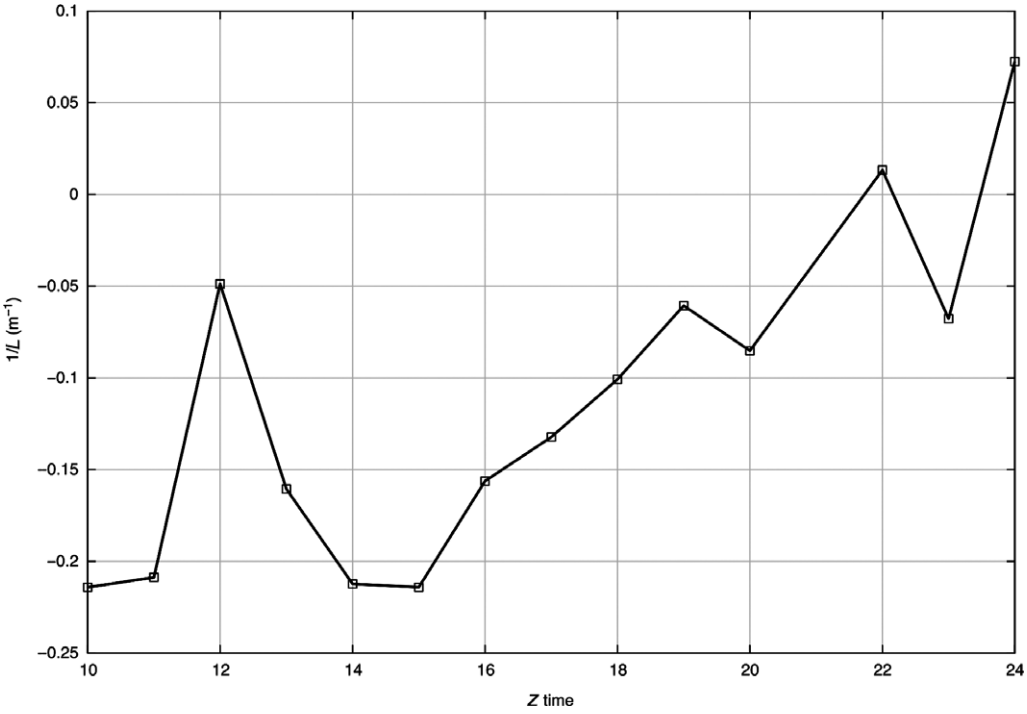

Figure 6. Time series of the measured surface Monin-Obukhov length during 20 June.

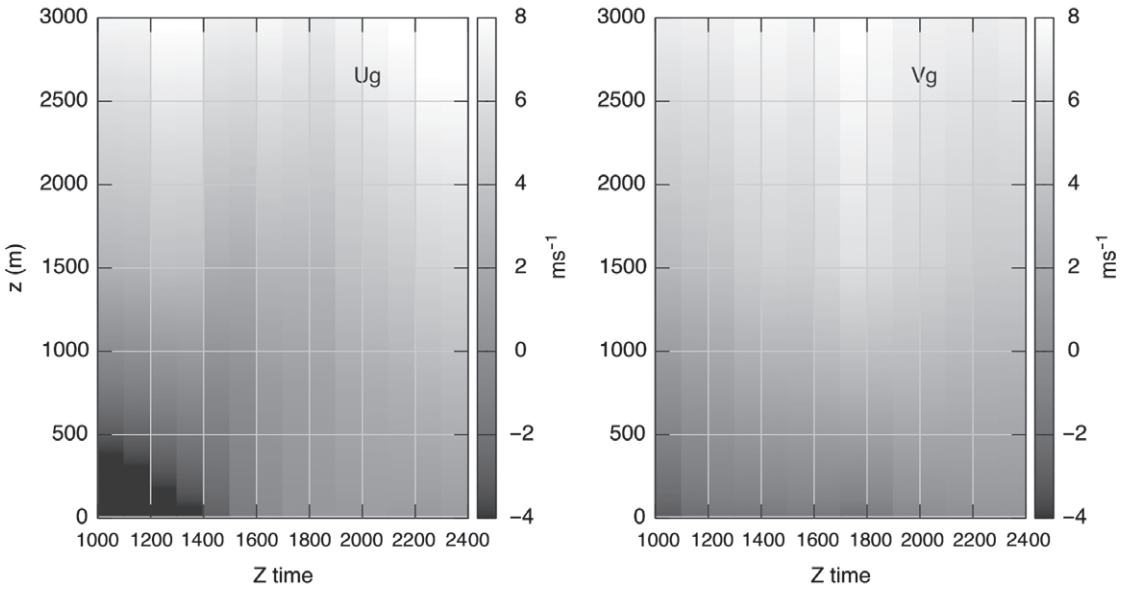

Figure 7. Time height plot of the geostrophic wind components during 20 June.

hand side of Equation (8) represents the additional terms in the LES equations.

For each flow variable (excluding the vertical component of wind and the subgrid turbulence kinetic energy) that is evaluated at a given time step, a horizontally averaged vertical profile $\overline{\Phi}(z)_{\mathrm{LES}}$ was calculated that was then compared with the corresponding experimental LASIE profile $\overline{\Phi}(z)_{\mathrm{LASIE}}$. This difference was then used as a restoring forcing term to be applied in the subsequent time step. In this context, through the force-restore term, the large-scale flow imposes a sort of control on the mean flow by preventing mean-flow profiles from deviating too much from their large-scale counterparts. On the other side, the turbulent flow features on scales smaller than the LES domain size are still reproduced by the turbulence mechanisms associated with the resolved and subgrid turbulent motions of LES.

4. Results and discussion

The reason for initializing the atmosphere with realistic environmental settings is to allow for a precise verification of LES output *via* atmospheric soundings. Verification is meaningful if the LES is capable of reproducing a variety of CBL features that may depend on the mesoscale situations. Here, the central issue is incorporating large-scale (as compared with the size of the LES domain) variability in LES. This is accomplished

in the present work in two ways. In the first simulation (named LES-NOFR) only the time varying baroclinic profiles are considered. In the second simulation (named LES-FR) a simple force-restore nudging technique is also added, that assumes the large-scale forcing is directly proportional to the deviation of horizontally averaged LES variables from their observed counterparts.

The test case that has been considered here is characterized by clear sky, calm sea, while the atmospheric stability alternated from slightly unstable to stable conditions (Sempreviva *et al.*, 2010). As shown in Figure 8, during 20 June the wind direction started to slowly rotated from 180 ° (south) to 240 ° (southwest), indicating an onshore wind blowing toward the Liguria coastline.

4.1. Surface values

Figure 9 shows the time series of virtual potential temperature (Figure 9(a)) and water vapour mixing ratio (Figure 9(b)) compared with observations. Surface observations show that during the simulated period a small virtual temperature decrease (2 K) occurs. As it can be easily seen, this behaviour is better reproduced with the simulation that uses the force-restore nudging. On the opposite, the LES-NOFR simulation has the opposite behaviour, showing an increasing virtual surface temperature.

During the whole simulated period the experimental value of the water vapour mixing ratio is almost constant (Figure 9(b)). The LES-FR again provides the best comparison, while the LES-NOFR has a linear decrease, which is not apparent in the experimental data. It is relevant to note that the initial conditions in LES-FR do not fit the observations exactly. In fact, the location of the buoy is not coincident with that of the vessel measuring the surface fluxes. Also, the surface values are derived from the observed fluxes by applying the Monin-Obukhov similarity theory and thus are inevitably approximate. However, the model outputs get progressively closer with time to the observed evolution as a consequence of the nudging.

These results indicate that, in order to simulate accurately surface temperature and water vapour mixing ratio, it is fundamental to include large-scale forcing within the LES.

4.2. Mean profiles

The development of the vertical structure of the MABL was monitored with radio-soundings launched from 2 m a.s.l. In Figures 10, 11, and 12, vertical profiles of water vapour mixing ratio, potential temperature and wind speed $(U^2 + V^2)^{1/2}$ are shown, taken respectively on 20 June at 1300 UTC (a), 1600 UTC (b), 1900 UTC (c) and finally 21 June at 0000 UTC (d).

In Figure 10 the comparison between the vertical profiles of water vapour mixing ratio is shown, as predicted by the two LES runs and the corresponding radio-soundings. Again a very good performance of the LES-FR run can be noted. The vertical profile of mixing ratio is well reproduced until the latest simulation time (Figure 10(a)–(d)), while the predictions of the LES-NOFR run are progressively degrading with time. In particular, the LES-FR run is able to reproduce the significant increase of mixing ratio with time, especially below 1000 m, which is not captured at all in the LES-NOFR run. The surface value, as measured with the ODASS buoy, is approximately constant at 14 g kg^{-1}: this is well reproduced in the LES-FR run, while LES-NOFR simulates a reduction from about 11 g kg^{-1} down to 8 g kg^{-1} in the course of the simulation.

In Figure 11, vertical profiles of potential temperature are shown. Again, the LES-FR simulation compares well qualitatively and quantitatively with the radiosoundings. The time evolution of the experimental profile reveals a ground-based inversion height that is increasing with time: for example, at 1900 UTC (Figure 11(c)) it is almost 200 m and almost 500 m

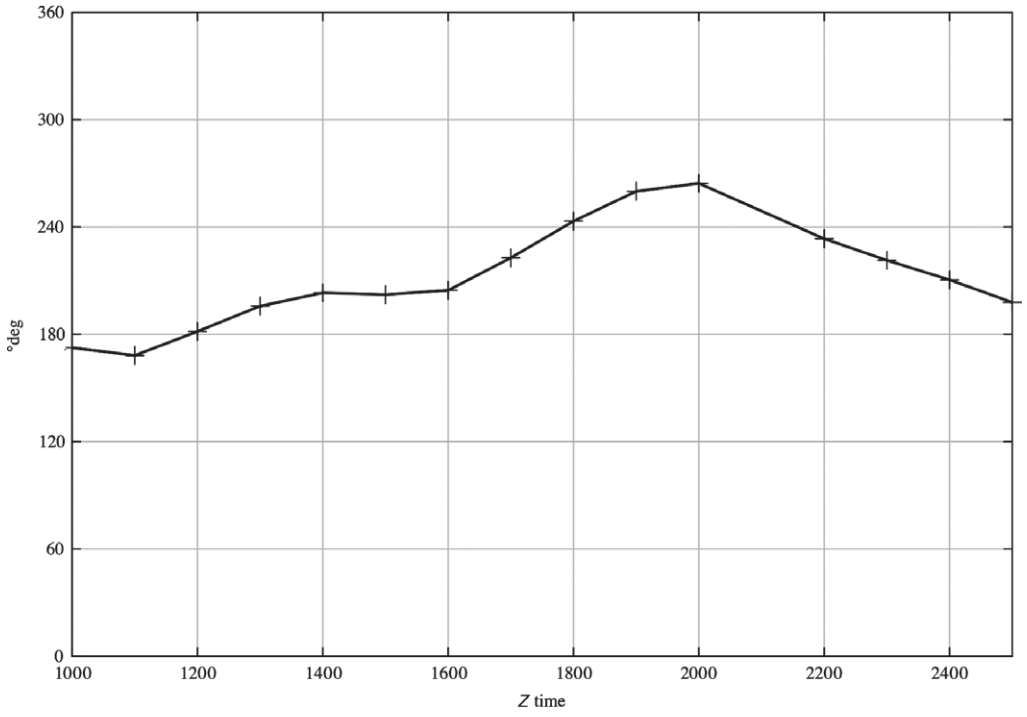

Figure 8. Time series of the wind direction during 20 June.

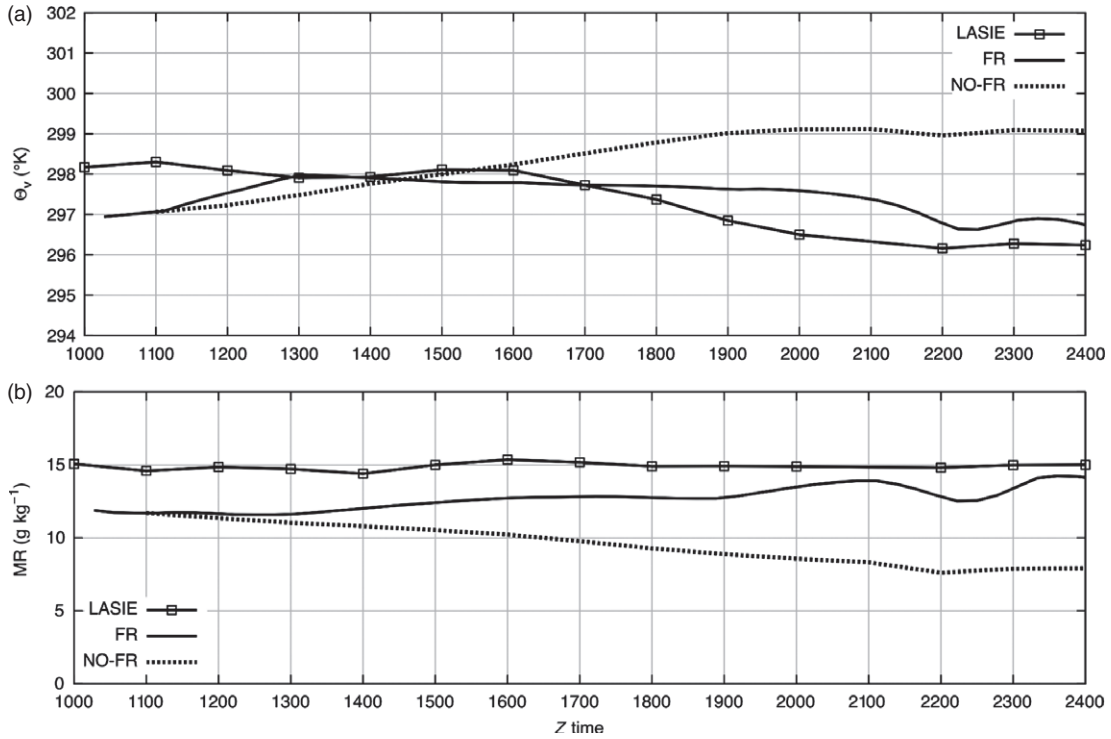

Figure 9. Time series of the surface virtual potential temperature (a) and water vapour mixing ratio (b) as predicted by LES-FR (continuous line), LES-NOFR (dotted) and compared with observations (continuous + square points).

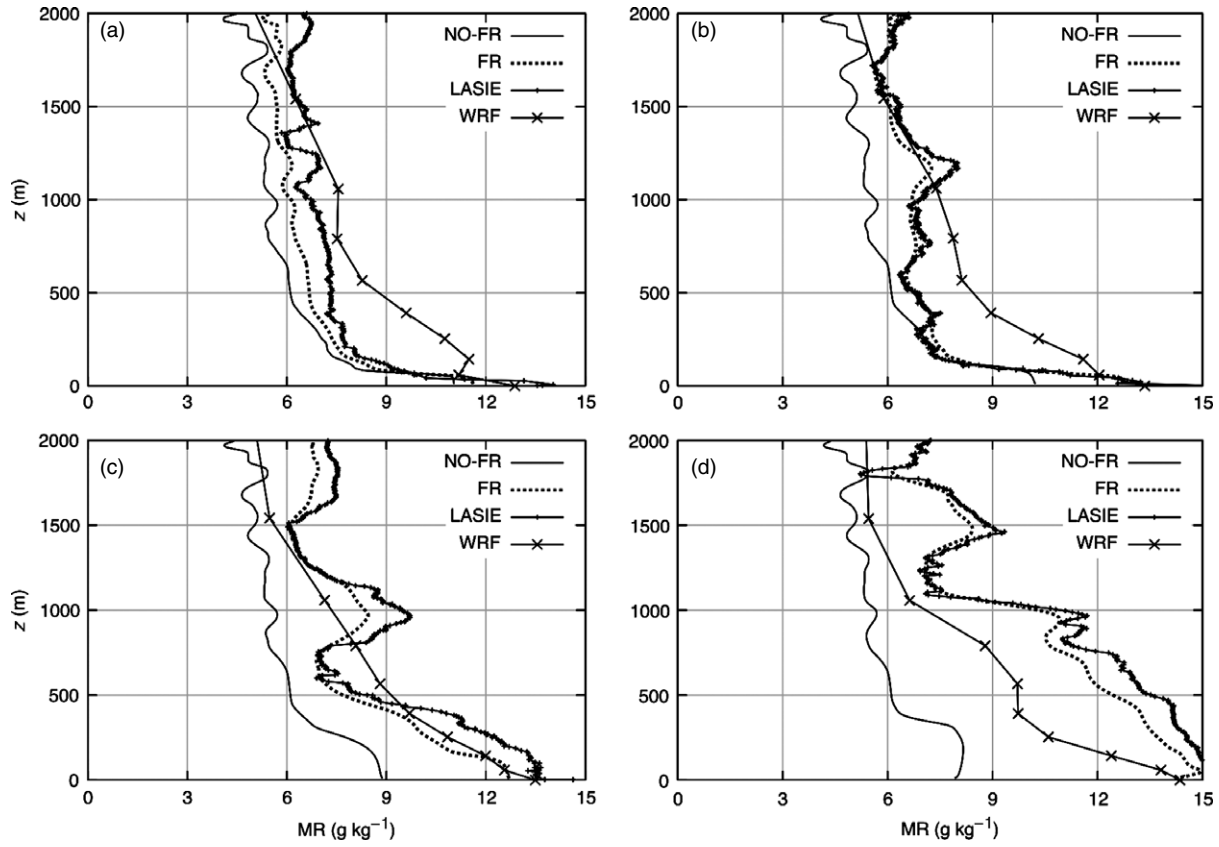

Figure 10. Vertical profiles of water vapour mixing ratio taken on 20 June, at 1300 UTC (a), 1600 UTC (b), 1900 UTC (c) and finally at 0000 UTC, 21 June (d), as predicted by LES-NOFR (continuous line), LES-FR (dotted) and compared with observations (continuous + square points) and WRF (continuous + cross points).

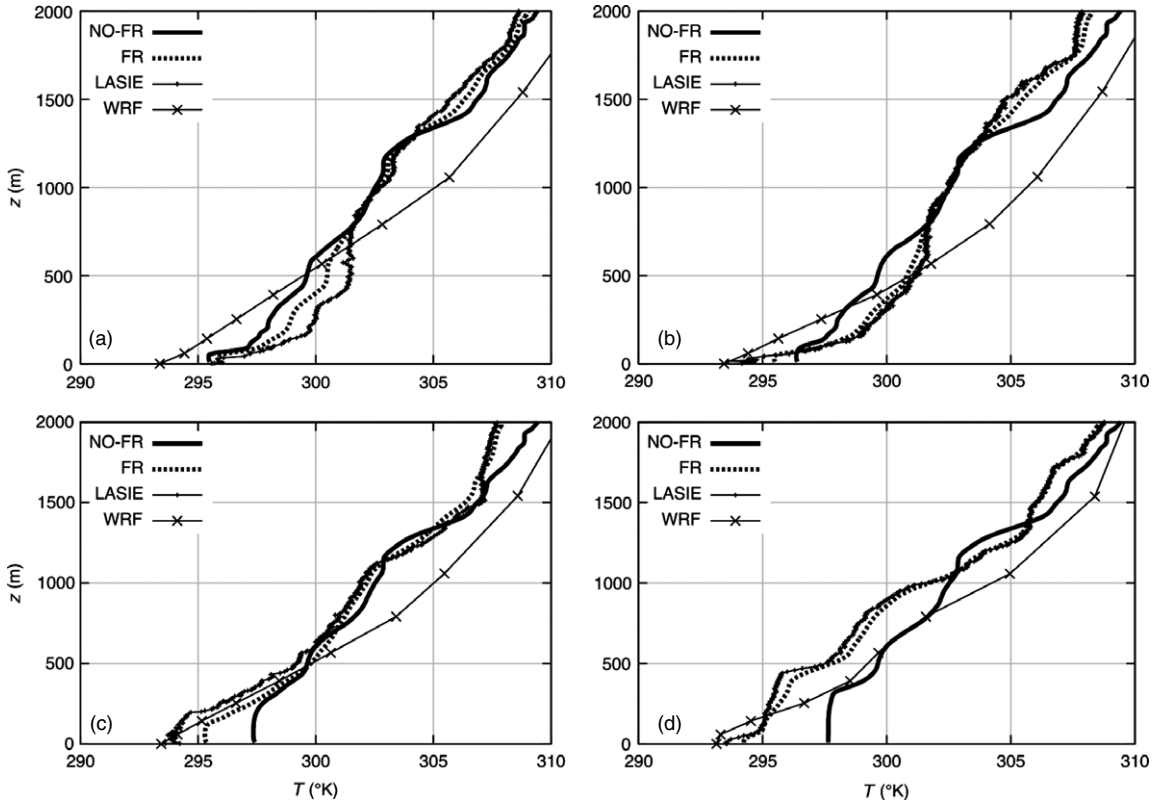

Figure 11. Vertical profiles of potential temperature mixing ratio taken on 20 June, at 1300 UTC (a), 1600 UTC (b), 1900 UTC (c) and finally at 0000 UTC, 21 June (d), as predicted by LES-NOFR (continuous line), LES-FR (dotted) and compared with observations (continuous + square points) and WRF (continuous + cross points).

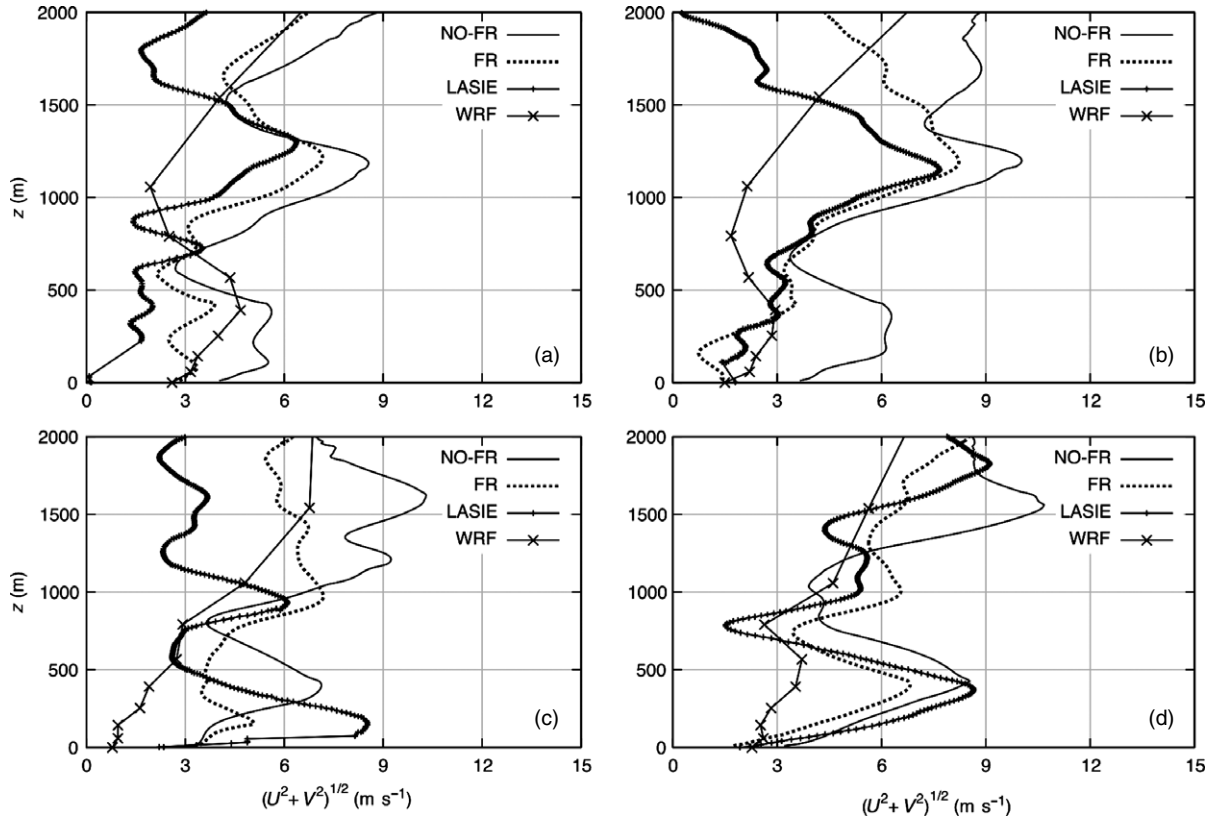

Figure 12. Vertical profiles of wind speed $(U^2 + V^2)^{1/2}$ taken at on 20 June, at 1300 UTC (a), 1600 UTC (b), 1900 UTC (c) and finally at 0000 UTC, 21 June (d), as predicted by LES-FR (continuous line), LES-NOFR (dotted) and compared with observations (continuous + square points) and WRF (continuous + cross points).

at 0000 UTC (Figure 11(d)). As can easily be seen, the LES-FR simulation reproduces this behaviour well. On the other hand, the LES-NOFR simulation has a performance degrading with time especially in the lowest 1000 m.

Finally, the vertical profiles of wind speed, $(U^2 + V^2)^{1/2}$, are shown in Figure 12. Again the LES-FR simulation has an overall better performance, although not so accurate as for the other fields. Starting at 1900 UTC (Figure 12(c)) experimental data show the formation of a low level jet with a maximum of 9 m s^{-1} at almost 400 m. It is relevant to note that the WRF model is not able to catch this feature, which is very challenging for limited area models. Anyway, both FR and NO-FR runs are able to correct this model limitation by identifying the presence of the low level jet pretty well.

In conclusion, the LES-FR outperforms the simulation without force-restore nudging for all the fields. This means that the evolution of the large-scale features needs to be incorporated into the model in order to provide a realistic evolution of the meteorological fields at local scale.

Figures 10, 11 and 12 also show the fields simulated in the WRF model run for the sake of comparison with the observed profiles and the two LES runs. It is apparent that, although the limited area model is able to reproduce the general features of the observed profiles, it performs worse than the two LES runs.

In particular, the fields are smoother and the WRF model is not able to catch some relatively small scale features, such as the low level jet (Figure 12(d)) and the inversion of potential temperature, respectively at 200 m in Figure 11(c) and at 500 m in Figure 11(d). In particular, its performance is worse for the wind and potential temperature fields. Conversely, WRF reproduces pretty well the profile of humidity, outperforming the LES-NOFR in the final part of the run.

5. Summary and conclusions

The growing interest for planning offshore wind farms and the need for an optimal exploitation of wind resources require the availability of numerical tools able to simulate wind conditions accurately. Unfortunately, the simulation of the mean and turbulent vertical structure of the Marine Atmospheric Boundary Layer (MABL) nearby coastal areas is very challenging, due to the coastline discontinuity with its strong horizontal gradients in surface characteristics. Also, the evolution of the vertical structure of the MABL is complex and is driven by an interplay of processes operating at different time and space scales, from microscale to synoptic scale, involving synoptic forcing, cloud cover, turbulence, that should be properly represented in a numerical model.

The innovative approach used here includes the implementation of a Large-Eddy Simulation model able to resolve turbulence at very high-resolution driven by the large-scale pressure gradient provided by a mesoscale meteorological model. The novelty consists in representing the large-scale forcing by additional terms in the LES equations. A simple force-restore nudging technique is used here, which assumes that the large-scale forcing is directly proportional to the deviation of the horizontally averaged LES variables from their observed counterparts, while the turbulent flow features on scales smaller than the LES domain size are left free to evolve, driven by turbulence mechanisms associated with resolved and subgrid turbulent motions directly reproduced by LES. The case study considered here is characterized by high pressure and stable conditions, from the LASIE campaign performed in the Ligurian Sea in summer 2007. During such a campaign, the MABL has been intensively monitored using different instrumentation devices installed on different measuring platforms, such as extensive ship- and buoy-based meteorological and oceanographic observations.

The results indicate that the realistic evolution of the surface fields as well as of vertical profiles at local scale require the inclusion of the large-scale forcing within the LES. In fact, the simulations including the external forcing outperform those without the force-restore nudging for all the fields. Thus, proper changes to the LES code may improve the prognostic ability of LES for offshore cases. Anyway, both LES runs improve significantly the simulation of vertical profiles with respect to the driving mesoscale model. LES appears as a promising technique to be applied to the simulation of offshore cases, particularly suitable for wind energy applications.

Nevertheless, the application of the force-restore nudging technique requires the availability of offshore data. Unfortunately there are only few available databases, generally limited to specific measurement campaigns. A way to bypass such a limitation is to use meteorological model fields as 'observations'. This strategy may open the way to a real-time application of the procedure.

However, the operational application of the force-restore technique must face with different limitations. A first drawback is the reliability of the meteorological models, which still suffer from limitations due to the inaccuracy of the initial conditions, especially at the mesoscale, and to their formulation, especially in terms of parameterization schemes. Actually, the meteorological models have significantly improved in the last few years, but still further refinements are necessary. Second, the LES requires a significant computational effort, due to the extremely high-resolutions employed, that needs several hours of computing time for a 1 day run. The progress in computational power will probably allow overtaking also this limitation in the future.

Acknowledgements

The Authors wish to thank Roberto Bozzano and Sara Pensieri from CNR/ISSIA for the ODAS 1 Buoy data. Funding from the FP6 ModObs Training Network within the Marie Curie Programme is acknowledged.

References

Anfossi D, Rizza U, Mangia C, Degrazia GA, Marques Filho EP. 2006. Estimation of the ratio between the Lagrangian and Eulerian time scales in an atmospheric boundary layer generated by Large Eddy simulation. *Bound.-Lay. Meteorol.* **120**: 25–37.

Antonelli M, Mazzino A, Rizza U. 2003. Statistics of temperature fluctuations in a buoyancy dominated boundary-layer flow simulated by a Large Eddy simulation model. *J. Atmos. Sci.* **60**: 215–224.

Barthelmie R, Hansen OF, Enevoldsen K, Hojstrup J, Frandsen S, Pryor S, Larsen S, Motta M, Sanderhoff P. 2005. Ten years of meteorological measurements for offshore wind farms. *J. Solar Energy Eng.* **127**: 170–177.

Basu S, Vinuesa JF, Swift A. 2008. Dynamic LES modeling of a diurnal cycle. *J. Appl. Meteorol. Climatol.* **47**: 1156–1174.

Cañadillas B, Neumann T, Raasch S. 2010. Getting a better understanding of the offshore marine boundary layer: comparison between Large Eddy Simulation and offshore measurement data with focus on wind energy application. *The 5th International Symposium on Computational Wind Engineering (CWE2010)*, 23–27 May, Chapel Hill, NC.

Conzemius RJ. 2004. The effects of wind shear on the convective boundary layer entrainment, PhD dissertation, University of Oklahoma, Norman, OK, 338 pp.

Conzemius RJ, Fedorovich E. 2008a. Simulations versus observations of a sheared convective boundary layer. *18th Symposium on Boundary Layers and Turbulence*, 9–13 June, Stockholm, Sweden.

Conzemius RJ, Fedorovich E. 2008b. A case study of convective boundary layer development during IHOP_2002: numerical simulations compared to observations. *Monthly Weather Rev.* **136**: 2305–2320.

Conzemius RJ, Fedorovich E. 2010. Large Eddy simulation of realistic wind fields in daytime atmospheric boundary layer. *The 5th International Symposium on Computational Wind Engineering (CWE2010)*, 23–27 May, Chapel Hill, NC.

De Tomasi F, Miglietta MM, Perrone MR. 2011. The growth of the PBL in a coastal site: a case study. *Bound.-Lay. Meteorol.* **139**: 521–541.

Edson J, Crawford T, Crescenti J, Farrar T, Frew N, Gerbi G, Helmis C, Hristov T, Khelif D, Jessup A, Jonsson H, Li M, Mahrt L, McGillis W, Plueddemann A, Shen L, Skyllingstad E, Stanton T, Sullivan P, Sun J, Trowbridge J, Vickers D, Wang S, Wang Q, Weller R, Wilkin J, Williams AJ III, Yue DKP, Zappa C. 2007. The coupled boundary layers and air-sea transfer experiment in low winds. *Bull. Am. Meteorol. Soc.* **88**: 341–356.

Garratt JR, Ryan BF. 1989. The structure of the stably stratified internal boundary layer in offshore flow over the sea. *Bound.-Lay. Meteorol.* **47**: 1–4.

Gibbs JA, Fedorovich E, Van Eijk AJ. 2011. Evaluating Weather Research and Forecasting (WRF) model predictions of turbulent flow parameters in a dry convective boundary layer. *J. Appl. Meteorol. Climatol.* **50**: 2429–2444.

Helmis CG. 2007. An experimental case study of the mean and turbulent characteristics of the vertical structure of the atmospheric boundary layer over the sea. *Meteorol. Z* **16**: 375–381.

Kalnay E, Kanamitsu M, Kistler R, Collins W, Deaven D, Gandin L, Iredell M, Saha S, White G, Woollen J, Zhu Y, Leetmaa A, Reynolds R, Chelliah M, Ebisuzaki W, Higgins W, Janowiak J, Mo KC, Ropelewski C, Wang J, Jenne R, Joseph D. 1996. The NCEP/NCAR 40-year reanalysis project. *Bull. Am. Meteorol. Soc.* **77**: 437–471.

Kumar V, Svensson G, Holtslag AAM, Meneveau C, Parlange MB. 2010. Impact of surface flux formulations and geostrophic forcing on Large Eddy simulations of diurnal atmospheric boundary layer flow. *J. Appl. Meteorol. Climatol.* **49**: 1496–1516.

Lange B, Larsen S, Højstrup J, Barthelmie R. 2004. The influence of thermal effects on the wind speed profile of the coastal marine boundary layer. *Bound.-Lay. Meteorol.* **112**: 587–617.

Miglietta MM, Zecchetto S, De Biasio F. 2013. A comparison of WRF model simulations with SAR wind data in a case study of orographic lee waves over the Eastern Mediterranean Sea. *Atmos. Res.* **120–121**: 127–146.

Moeng C-H. 1984. A Large-Eddy-simulation model for the study of planetary boundary-layer turbulence. *J. Atmos. Sci.* **41**: 2052–2062.

Moeng C-H, Sullivan PP. 1994. A subgrid-scale model for Large-Eddy simulation of planetary boundary-layer flows. *Bound.-Lay. Meteorol.* **71**: 247–276.

Nittis K, Tziavos C, Bozzano R, Cardin V, Thanos Y, Petihakis G, Schiano ME, Zanon F. 2007. The M3A multi-sensor buoy network of the Mediterranean Sea. *Ocean Sci.* **3**: 229–243.

Pedersen JG, Kelly M, Gryning SE, Floors R, Batcharova E, Pena A. 2012. Comparison of Large Eddy simulations of a convective boundary layer with wind LIDAR measurements. *Adv. Sci. Res.* **8**: 83–86.

Pryor SC, Barthelmie RJ. 2002. Statistical analysis of flow characteristics in the coastal zone. *J. Wind Eng. Ind. Aerodyn.* **90**: 201–221.

Rizza U, Degrazia GA, Mangia C, Marques Filho EP. 2010. Estimation of the kolmogorov constant for the lagrangian velocity spectrum and structure function under different PBL stability regimes generated by LES. *Physica A* **389**: 4009–4017.

Rizza U, Miglietta MM, Acevedo O, Anabor V, Degrazia GA, Goulart AG, Zimmerman HR. 2013. Large-Eddy simulation of the planetary boundary layer under baroclinic conditions during daytime and sunset turbulence. *Meteorol. Appl.* **20**: 56–71.

Saiki EM, Moeng C-H, Sullivan PP. 2000. Large-Eddy simulation of the stably stratified planetary boundary layer. *Bound.-Lay. Meteorol.* **95**: 1–30.

Sempreviva AM, Gryning SE. 2000. Mixing height over water and its role on the correlation between temperature and humidity fluctuations in the unstable surface layer. *Bound.-Lay. Meteorol.* **97**: 273–291.

Sempreviva AM, Schiano ME, Pensieri S, Semedo S, Tome R, Bozzano R, Borghini M, Grasso F, Soerensen LL, Teixeira J, Transerici C. 2010. Observed development of the vertical structure of the marine boundary layer during the LASIE experiment in the Ligurian Sea. *Ann. Geophys.* **28**: 17–25.

Skamarock WC, Klemp JB, Dudhia J, Gill DO, Barker DM, Duda M, Huang XY, Wang W, Powers JA. 2008. *A Description of the Advanced Research WRF Version 3*, Technical Note TN- 475 STR. Boulder, CO.: NCAR.

Skyllingstad ED, Samelson RM, Mahrt L, Barbour P. 2005. A numerical modeling study of warm offshore flow over cool water. *Monthly Weather Rev.* **133**: 345–361.

Small RJ, Campbell T, Teixeira J, Carniel S, Smith TA, Dykes J, Chen S, Allard R. 2011. Air–sea interaction in the ligurian sea: assessment of a coupled ocean–atmosphere model using in situ data from LASIE07. *Monthly Weather Rev.* **139**: 1785–1808.

Smedman AS, Hogstrom U, Hunt JCR, Salee E. 2007. Heat/mass transfer in the slightly unstable atmospheric surface layer. *Q. J. R. Meteorol. Soc.* **133**: 37–51.

Stevens B, Moeng C-H, Ackerman AS, Bretherton CS, Chlond A, de Roode S, Edwards J, Golaz J-C, Jiang H, Khairoutdinov M, Kirkpatrick MP, Lewellen DC, Lock A, Müller F, Stevens DE, Whelan E, Zhu P. 2005. Evaluation of Large-Eddy simulations via observations of nocturnal marine stratocumulus. *Monthly Weather Rev.* **133**: 1443–1462.

Sullivan PP, Edson JB, Hristov T, McWilliams JC. 2008. Large-Eddy simulations and observations of atmospheric marine boundary layers above nonequilibrium surface waves. *J. Atmos. Sci.* **65**: 1225–1245.

Teixeira J. 2007. *Ligurian Air-Sea Interaction Experiment (LASIE) Trial Plan*. NATO Undersea Research Centre, La Spezia, Italy; 30 pp. http://geos2.nurc.nato.int/mreaconf/ppt/3.0.pdf (accessed 22 July 2013).

Weckwerth TM, Parsons DB, Koch SE, Moore JA, LeMone MA, Demoz BB, Flamant C, Geerts B, Wang J, Feltz WF. 2004. An overview of the International H2O Project (IHOP_2002) and some preliminary highlights. *Bull. Am. Meteorol. Soc.* **85**: 253–277.

